Response of bubbles to diagnostic ultrasound: a unifying theoretical approach

S. Hilgenfeldt[1,a], D. Lohse[1,b], and M. Zomack[2]

[1] Fachbereich Physik der Universität Marburg, Renthof 6, 35032 Marburg, Germany
[2] Schering AG, Clinical Development, Müllerstr. 178, 13342 Berlin, Germany

Abstract. The scattering of ultrasound from bubbles of $\sim 1\ \mu$m radius, such as used in contrast enhancers for ultrasound diagnostics, is studied. We show that sound scattering and "active" emission of sound from oscillating bubbles are not contradictory, but are just two different aspects derived from the same physics. Treating the bubble as a nonlinear oscillator, we arrive at general formulas for scattering and absorption cross-sections. We show that several well-known formulas are recovered in the linear limit of this ansatz. In the case of strongly nonlinear oscillations, however, the cross-sections can be larger than those for linear response by several orders of magnitude. The major part of the incident sound energy is then converted into emitted sound, unlike what happens in the linear case, where the absorption cross-sections exceed the scattering cross-sections.

PACS. 87.59.Mt Ultrasonography – 43.80.+p Bioacoustics – 43.25.+y Nonlinear acoustics, macrosonics

1 Introduction

In recent years, a new kind of contrast agent for use in ultrasound diagnostics has been developed: suspensions of gas filled microbubbles, *i.e.*, bubbles of at most a few micrometers in diameter [1]. The enhancement of image brightness and contrast is mostly due to the well-known fact that microbubbles of this size can have tremendous scattering cross-sections for the incident diagnostic ultrasound (with frequencies around $1-10$ MHz) [2]. A number of different theoretical approaches are present in literature, resulting in formulas for the scattering and absorption cross-sections that do not always seem compatible (see *e.g.* [1,3–5]). It is one of the main goals of this work to show that all of these results can be understood as special cases of a unified approach which treats the bubble as a (generally nonlinear) volume oscillator. The different appearance in literature is only due to the use of different formalisms (*e.g.* full-fledged scattering theory with partial wave decomposition [5] or linear oscillator theory [4]) and the validity of different limiting cases (*e.g.* neglecting surface tension [1,3]).

The other main goal of our present study is to go beyond previous work [6], where monochromatic driving was treated, and employ *pulsed* driving within our formalism, in order to achieve a more realistic modeling of the situation in diagnostic applications. The analysis of the emitted sound from the bubbles in terms of intensity and spectral distribution is of obvious importance to assess the signal quality of ultrasonography with bubble contrast agents. While a large number of publications have dealt with the sound emission of *linearly* oscillating bubbles (see *e.g.* [4,5] and references therein), and the *weakly* nonlinear case was treated by Prosperetti [7,8], a systematic study of cross-sections for *strongly nonlinear* response to *pulsed* driving has, to our knowledge, not yet been performed. It is this fully nonlinear case of bubble oscillations which is encountered in ultrasound diagnostics as driving pressure amplitudes of up to ~ 10 atm are common, whereas strong nonlinearities occur already for amplitudes $\lesssim 1$ atm.

We present our general, unifying approach in Section 2 and show in Section 3 how it translates to a multitude of linear limiting cases, where analytical results can be obtained if monochromatic driving is assumed. Still in the linear limit, we then introduce pulsed driving in Section 4 and finally present results for the full nonlinear case in Section 5. A more detailed discussion, especially of spectral properties of the emitted sound for nonlinear response, will be postponed to another publication [9]. Section 6 presents conclusions.

[a] *Present address:* Division of Engineering and Applied Sciences, Harvard University, 29 Oxford St., Cambridge, MA 02138, USA; e-mail:sacha@stockes.harvard.edu
[b] *Present address:* University of Twente, Applied Physics, Postbus 217, 7500 AE Enschede, The Nederlands; e-mail: lohse@utwente.nl

2 Sound emission and absorption

2.1 Emitted sound pressure

We want to evaluate the pressure of emitted sound $P_s(r,t)$ from a body capable of volume oscillations (*i.e.*, a bubble) driven by an incident pressure wave $P(t)$. First, we notice that there are two contributions to $P_s(r,t)$:

(i) the *active emission* of sound, caused by the change of volume of the body, and;
(ii) the *passive* contribution due to the mere presence of the (maybe non-oscillating) body in the incident field.

Thus, we can write

$$P_s(r,t) = P_s^a(r,t) + P_s^p(r,t). \qquad (1)$$

For a body of volume $V_b(t)$ which is much smaller than the wavelength of the incident sound, the pressure $P_s^a(r,t)$ of *actively emitted* sound is given to leading order by [3,10]

$$P_s^a(r,t) = \frac{\rho_l}{4\pi r} \frac{d^2 V_b}{dt^2}. \qquad (2)$$

Here, ρ_l is the liquid density and we have adopted a spherical coordinate system with radius r. There is no angular dependence because we have assumed the long wavelength limit (S wave scattering). For a spherical bubble with radius dynamics $R(t)$, (2) easily translates to

$$P_s^a(r,t) = \rho_l \frac{R(t)}{r} \left(2\dot{R}(t)^2 + R(t)\ddot{R}(t) \right) = \frac{1}{r} q_s^a(t), \qquad (3)$$

where we have introduced $q_s^a(t) \equiv r P_s^a(r,t)$, thus separating the trivial (geometrical) $1/r$ spatial dependence of the radiation from the time-dependent part.

The second term $P_s^p(r,t)$ in (1) is the pressure of *passively* emitted sound due to the mere presence of the body. It arises from the perturbation of the density field in water: if the body was not present, the incident sound wave could induce density changes in the volume of liquid occupied by the body. As this cannot happen, the situation is equivalent to having an oscillator that compensates the effects of the sound wave; this oscillator has a (virtual) volume change

$$\frac{dV}{dt} = V_0 \frac{d\rho_l/dt}{\rho_l}, \qquad (4)$$

with the (now constant) volume V_0 of the body, see [3]. For a sound wave $P(t)$, we have $dP/d\rho_l = c_l^2$, where the derivative is taken at constant entropy. Then, in analogy to (2), replacing V_b by V and inserting $V_0 = 4\pi R^3/3$, we get the leading order pressure change due to the passive reaction to the sound wave

$$P_s^p(r,t) = \frac{1}{3rc_l^2} R^3(t) \ddot{P}(t) = \frac{1}{r} q_s^p(t), \qquad (5)$$

where c_l is the speed of sound in the liquid. Note again that we are in the limit $R(t) \ll \lambda$, where λ is the wavelength of incident sound. Therefore, the driving pressure $P(t)$ can be treated as spatially uniform, *i.e.*, the pressure experienced by the bubble does not vary over its size. In analogy to (3), we have defined the quantity $q_s^p(t)$.

2.2 Bubble oscillation

To evaluate (3) or (5), we need a formula for $R(t)$. The oscillatory behavior of the radius R of a gas bubble in a liquid is well described by the Rayleigh-Plesset equation [11,10]. Many variants of this equation have been presented (see *e.g.* [12–18]); the following form has proved to be robust and close to experiment even in situations of massively nonlinear bubble behavior, as *e.g.* in sonoluminescence experiments [19]:

$$R\ddot{R} + \frac{3}{2}\dot{R}^2 = \frac{1}{\rho_l} \left(p(R,t) - P(t) - P_0 \right)$$
$$+ \frac{R}{\rho_l c_l} \frac{d}{dt} p(R,t) - 4\nu_l \frac{\dot{R}}{R} - \frac{2\zeta}{\rho_l R}. \qquad (6)$$

We have introduced the liquid viscosity ν_l and surface tension ζ here, as well as the ambient pressure P_0 taken to be 1 atm in this work. All liquid parameters assume the values of water, except for ν_l, which is multiplied by three to mimic the viscosity of blood [20]. $p(R,t)$ stands for the gas pressure *inside* the bubble and is modeled by a polytropic process equation with van der Waals hard core and parameters for air. The polytropic exponent is taken to be one, because bubbles of the sizes we treat here ($\sim 1~\mu$m) are smaller than the thermal diffusion length on the time scales of the oscillation, and can therefore be regarded as isothermal [21,22].

2.3 Scattering cross-sections

In general, the scattering cross-section σ_{sc} is related to the incident intensity (energy/area/time) I_{inc} and the scattered power W_{sc} (energy/time) *via*

$$W_{sc} = \sigma_{sc} I_{inc}, \qquad (7)$$

and has thus the dimensions of an area. I_{inc} is determined by the incident pressure wave $P(t)$, namely (see, *e.g.*, [3], §65)

$$I_{inc} = \frac{1}{\rho_l c_l} \langle P^2(t) \rangle_t \qquad (8)$$

and W_{sc} follows from $P_s(r,t)$ through

$$W_{sc} = \frac{4\pi}{\rho_l c_l} \langle r^2 P_s^2(r,t) \rangle_t = \frac{4\pi}{\rho_l c_l} \langle q_s^2(t) \rangle_t. \qquad (9)$$

Here, $\langle \cdot \rangle_t$ denotes a time mean; we have exploited the virial theorem to express intensities and powers solely in terms of pressures (the "potential" part of the energy of the wave). The integral

$$E_{sc} = \frac{4\pi}{\rho_l c_l} \int_0^\tau q_s^2(t) \, dt \qquad (10)$$

gives the total scattered energy over a time span τ (*e.g.* the duration of an incident sound pulse).

From these definitions, it is clear that the general formula for the scattering cross-section is

$$\sigma_{sc} = \frac{4\pi}{\langle P^2(t)\rangle_t}\langle q_s^2(t)\rangle_t = \frac{4\pi}{\langle P^2(t)\rangle_t}\langle [q_s^a(t) + q_s^p(t)]^2\rangle_t. \tag{11}$$

We notice that the active and passive parts *interfere*. It is therefore, strictly speaking, wrong to divide σ_{sc} into an active and a passive part, as it is sometimes done in literature. Nevertheless, it will be shown below that in the case of diagnostic bubbles the total scattering cross-section is almost exclusively due to the active part P_s^a of (1), while the passive contribution can safely be neglected.

There are other possible contributions to $P_s(r,t)$, *e.g.* direct or indirect results of bubble shape oscillations. These are not analyzed here because perfect sphericity is assumed. Also, there is a contribution if the bubble (or the body in general) can be translated as a whole by the incident sound. This term is orthogonal to those treated above (*i.e.*, the interference terms vanish) and results in a well-defined *additional* scattering cross-section (*cf.* [3] §78 or [1]) with a characteristic angular dependence. As it is (for the case of a gas bubble in a liquid) always of the same order of magnitude as the passive contribution, and is therefore equally negligible, we do not treat it here in detail. Finally, if two or more bubbles come close to each other, they will change the emitted sound field either by direct secondary scattering or indirectly by modifying their modes of oscillation (*e.g. via* secondary Bjerknes forces [23,24]). We will not try to incorporate these effects, but restrict ourselves to the case of a single bubble.

2.4 Absorption cross-section

We have so far regarded the scattering cross-section as an indicator of the acoustic energy deflected by the scatterer. Likewise, the absorption cross-section σ_{abs}^ν stands for the energy loss induced by the viscous term in the RP equation (6). In this case the energy is directly converted into heat and will, in general, be of little use to the experimenter, whereas the scattered sound can be detected much more easily. Nevertheless, σ_{abs}^ν is important in order to assess the energy balance of the scattering process. The liquid viscosity exerts a stress

$$p_{vis} = \frac{4\nu_l\rho_l\dot{R}}{R} \tag{12}$$

over the bubble surface of size $A = 4\pi R^2$ (this can be read off directly from the RP equation). As the bubble wall moves with velocity $\dot{R}$, the dissipated power is

$$W_{dis}^\nu = p_{vis}A\dot{R} = 16\pi\nu_l\rho_l R\dot{R}^2. \tag{13}$$

The absorption cross-section is determined in analogy to σ_{sc} *via*

$$W_{dis}^\nu = \sigma_{abs}^\nu I_{inc}. \tag{14}$$

3 Small driving: the linear case

The formulas given in the previous sections can be applied to all cases of bubble motion and subsequent sound emission. For small driving, they reduce to the linear case and almost all quantities can be calculated analytically. First of all, the RP equation can be linearized: we set $R(t) = R_0(1 + x(t))$ (R_0 is the radius of the undriven bubble under ambient conditions) and get

$$\ddot{x} + 2\gamma\dot{x} + \omega_0^2 x = \frac{P(t)}{\rho_l R_0^2} \tag{15}$$

with the viscous damping constant $\gamma = \dfrac{2\nu_l}{R_0^2}$ and the bubble eigenfrequency

$$\omega_0^2 = \frac{3\kappa_g P_0}{\rho_l R_0^2} + \frac{4\zeta}{\rho_l R_0^3}. \tag{16}$$

This latter quantity consists of two distinct terms, the first due to the gas pressure $p(R,t)$, and the second governed by surface tension ζ. For $p(R,t)$, a polytropic ideal gas formula was chosen. While it is advisable to employ a more elaborate formula (*e.g.* a van der Waals gas with hard core) if the bubble oscillation is violent, the ideal gas is a very good approximation in the linear limit. The polytropic exponent κ_g measures the gas compressibility ($p(R,t) \propto \rho_g^{\kappa_g}$); it is 1 for isothermal behavior and equal to the adiabatic exponent for adiabatic behavior of an ideal gas (*e.g.* 7/5 for air). In deriving equation (15), we note that effects of thermal damping are neglected (as they have not been present in (6), either), and also radiation damping (caused in (6) by the term involving c_l) is not present. Both of these damping effects are very small in the parameter range of our interest; thus, γ only contains viscous damping contributions.

To get explicit solutions, let us assume monochromatic driving $P(t) = P_a \cos\omega_d t$ in (15). P_a is the driving pressure amplitude, $\omega_d = 2\pi f_d$ the angular driving frequency. This yields

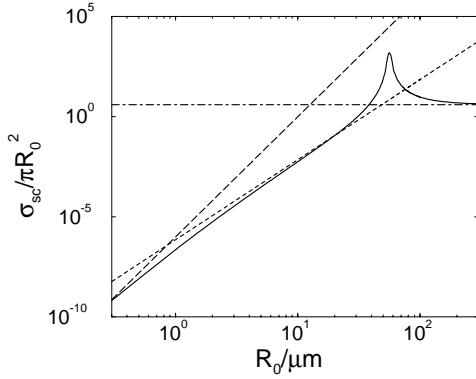$$x(t) = \varepsilon\cos(\omega_d t + \delta) \tag{17}$$

with the amplitude

$$\varepsilon = -\frac{P_a}{\rho_l R_0^2}\frac{1}{\sqrt{(\omega_0^2 - \omega_d^2)^2 + 4\gamma^2\omega_d^2}}, \tag{18}$$

and the phase shift

$$\delta = \arctan\left(\frac{2\gamma\omega_d}{\omega_d^2 - \omega_0^2}\right). \tag{19}$$

Obviously, in the monochromatic case $I_{inc} = \dfrac{P_a^2}{2\rho_l c_l}$. With $R(t)$ from $x(t)$, equations (3, 5, 11) we get

$$\sigma_{sc}^{lin} = 4\pi R_0^2\left\langle\left[\frac{\sqrt{2}\omega_d^2\cos(\omega_d t + \delta)}{\sqrt{(\omega_0^2 - \omega_d^2)^2 + 4\gamma^2\omega_d^2}} - \frac{\sqrt{2}}{3c_l^2}R_0^2\omega_d^2\cos\omega_d t\right]^2\right\rangle_t. \tag{20}$$

Fig. 1. Numerical computation (solid line) and scaling behaviors of the normalized scattering cross-section for bubbles driven with a monochromatic 50 kHz sound wave at small drive amplitudes (linear case). We chose a representation similar to that of Nishi [5], displaying σ_{sc} divided by the geometrical cross-section πR_0^2 on a double logarithmic plot. To the right of the resonance peak (for large R_0), $\sigma_{sc}/(\pi R_0^2)$ relaxes to 4 (dot-dashed line). In the opposite limit of small R_0, it scales $\propto R_0^4$ (dashed) for an interval, but becomes steeper again for very small R_0, reaching an asymptote $\propto R_0^6$ (long dashed). These scaling laws correspond to the R_0^6 and R_0^8 behaviors of the unnormalized σ_{sc}, respectively (cf. Eqs. (23, 24)).

Note that σ_{sc}^{lin} does not depend on the absolute size of P_a, as long as the oscillation stays linear. Fortunately, in all cases of interest to bubble ultrasound diagnostics, i.e., for frequencies in the MHz range and R_0 between a few tenths of a micron and a few microns, the second (passive) term of this formula is negligible compared to the first (active) part. We will show in detail below that the dominance of the active emission is so overwhelming that the relative errors in neglecting the passive contribution never exceed 0.25% in the parameter range of this study. Dropping the passive term, we get the considerably simplified expression (reproducing results presented e.g. in Leighton [4] in Sect. 4.1)

$$\sigma_{sc}^{lin} \approx 4\pi R_0^2 \frac{\omega_d^4}{(\omega_0^2 - \omega_d^2)^2 + 4\gamma^2\omega_d^2}. \qquad (21)$$

This formula can also be translated into the S wave scattering limit of the complete scattering analysis by Nishi [5]. In equation (47) of that work, there are additional contributions to γ due to thermal and radiation damping, as well as modifications involving the stiffness of the bubble. In certain limiting cases, (21) gets further simplified. Moreover, a rich variety of scaling behaviors, especially in R_0, can be found. The richness (as compared to "ordinary" linear oscillators) is due to the fact that in (15), the damping, driving frequency and dimensionless driving all depend on R_0. In Figure 1 σ_{sc}^{lin} is presented for a 50 kHz-driven bubble, a frequency chosen such that most of the limiting cases treated in the following subsections can be illustrated by the graph. Note that all cross-section graphs in this work were computed with the full numerical formulas presented in Section 2.

3.1 Small bubbles: dominance of gas pressure or surface tension

For small bubbles (such that $\omega_0 \gg \omega_d$) the denominator of the active contribution in (20) simplifies to ω_0^2. It is crucial here to verify which of the two contributions to ω_0 in (16) is dominant. If surface tension is very small (and R_0 is not extremely tiny), ω_0 will be governed by the first term, i.e., the one due to the internal gas pressure. With the polytropic ansatz, we can use $c_g^2 = \kappa_g P_0/\rho_g$ for the speed of sound in the gas c_g and from (20) the limiting behavior for small R_0 is then

$$\sigma_{sc}^{lin} \to \frac{4\pi}{9} \frac{R_0^6 \omega_d^4}{c_l^4} \left(1 - \frac{K_g}{K_l}\right)^2 \qquad (22)$$

with the compressibilities $K_i = 1/(\rho_i c_i^2)$ for the bubble interior ($i = g$) and exterior ($i = l$). This reproduces the equations presented e.g. by Landau [3] §78, deJong [25] or Meerbaum in Nanda/Schlief [1] (apart from the translational contribution mentioned in Sect. 2.3 above). Note that in the case of gas bubbles in a liquid, K_g will be much greater than K_l, so that to very good approximation

$$\sigma_{sc}^{lin} \to \frac{4\pi}{9} \frac{R_0^6 \omega_d^4}{c_l^4} \left(\frac{K_g}{K_l}\right)^2 \qquad (23)$$

and the dominance of the active scattering is again confirmed. In fact, as for typical materials $\rho_l \approx 1000\rho_g$ and $c_l \approx 5c_g$, the active emission can surmount what would be expected from a purely passive scatterer by more than eight orders of magnitude! This is why oscillating bubbles are so much superior to (completely passive) hard spheres in terms of ultrasound scattering capability. In Figure 1 there is indeed a region where the $\propto R_0^6$ behavior of σ_{sc}^{lin} is observed. Note, however, that the validity of equations (22, 23) for bubbles is limited, especially as surface tension is explicitly neglected.

If surface tension is taken into account and the parameters for water are inserted into (16), we see that for $R_0 \leq 0.96$ μm the surface tension term dominates ω_0, so that $\omega_0^2 \to 4\zeta/\rho_l R_0^3$. As a consequence, the active scattering cross-section will acquire a different limit, namely

$$\sigma_{sc}^{lin} \to \frac{\pi R_0^8 \omega_d^4 \rho_l^2}{4\zeta^2}. \qquad (24)$$

The steeper $\propto R_0^8$ behavior takes over in Figure 1 for very small bubbles, as expected. As the passive contributions scale like R_0^6, there has to be a (small) radius where the latter become dominant. This radius is easily calculated to be

$$R_0^p = \frac{4\zeta}{3\rho_l c_l^2}, \qquad (25)$$

which, for the material constants of the water/air (blood/air) system, is $\approx 4.4 \times 10^{-11}$ m, i.e., on a subatomic scale which is not described by the physics discussed here.
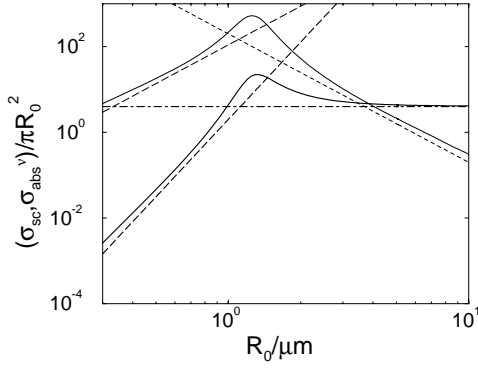
Fig. 2. Numerical computation (solid lines) and scaling behaviors of the normalized linear scattering (thick lines) and absorption (thin lines) cross-sections for bubbles driven with a monochromatic 3 MHz sound wave (diagnostic frequency). The resonance features as well as the large R_0 limit of 4 (dot-dashed) are again present in $\sigma_{sc}/(\pi R_0^2)$. Of the small R_0 limits, only the surface tension governed $\sigma_{sc}^{lin} \propto R_0^8$ remains (long dashed). The corresponding scaling laws for $\sigma_{abs}^{\nu,lin}/(\pi R_0^2)$ are $\propto R_0^{-1}$ (dashed) for large and $\propto R_0^5$ (long dashed) for small R_0.

3.2 Linear resonance

When R_0 is such that $\omega_0 \sim \omega_d$, the bubble is near resonance, *i.e.*, its oscillation amplitude ϵ and thus σ_{sc}^{lin} become much larger than for neighboring R_0. E.g., for the case of air bubbles in blood driven with $\omega_d = 2\pi \times 3\,\mathrm{MHz}$, it reaches values of about 15 times the geometrical cross-section πR_0^2 (*cf.* Fig. 2), *i.e.*, the normalized cross-section $\sigma_{sc}^{lin}/(\pi R_0^2)$ is larger than for any other radius. From (21), it is easy to get

$$\sigma_{sc}^{lin,res} \approx \frac{\pi (R_0^{res})^6 \omega_d^2}{4\nu_l^2}, \qquad (26)$$

where R_0^{res} is determined by the condition $\omega_0(R_0^{res}) = \omega_d$. The height of the resonance peak is thus mainly determined by the strength of damping, *i.e.*, the viscosity of the liquid. In water with its three times lower viscosity, the maximum cross-section is therefore 9 times higher than in blood. The (Lorentz shaped) resonance peak is the hallmark of the classical pictures of linear bubble scattering cross sections (see [1,4,5]). We will see that this shape changes considerably in the nonlinear case.

3.3 Large bubbles: the "soft sphere" limit

For large bubbles (but still obeying $R \ll \lambda$), $\omega_d \gg \omega_0$ and

$$\sigma_{sc}^{lin} \to 4\pi R_0^2, \qquad (27)$$

i.e., the scattering cross-section becomes four times the geometrical cross-section, which is also reproduced in Figure 1. Equation (27) describes the behavior for *all* R_0 if the bubble interior is arbitrarily *compressible* while surface tension is absent ($\zeta = 0$). This can be seen if we imagine $\kappa_g \to 0$ (implying $c_g \to 0$ and $K_g \to \infty$) and thus $\omega_0 \to 0$:

the resonance peak is shifted to very small R_0 and every larger ambient radius results in the "soft sphere limit" cross-section (27).

In reality, for large bubbles there are of course still the interference contributions with the passive term $\propto R_0^6$. But the influence of P_s^p can only outweigh the active emission for $R_0 > \frac{\sqrt{3}}{2\pi}\lambda$ (which is again easy to prove); this is already in a region where the assumption $R_0 \ll \lambda$ is dubious. In fact, for diagnostic ultrasound with $\omega_d = 2\pi \times 3\,\mathrm{MHz}$, $\lambda \approx 500\,\mu\mathrm{m}$, resulting in a critical radius for passive influence of $R_0 \lesssim 140\,\mu\mathrm{m}$. Thus, there is at most a very small region of transition until the scattering cross-section has to be described by completely different formulas (Mie scattering theory), and the bubbles in this region are of no interest to ultrasound diagnostics because of their size.

3.4 Other limits

There are a number of limiting cases of equations (20, 21) that go beyond the parameter space of this study; they are given here for completeness:

- In the limit of $R_0 \gg \lambda$, the cross-section relaxes to the limit $\sigma_{sc} = 2\pi R_0^2$ [5]. This is only relevant for mm-sized or even larger bubbles.
- If we apply our formulas to solid spheres in a liquid rather than bubbles, *i.e.*, we make the interior of the "bubble" much more stiff than the liquid, the main contribution in (22) is the *passive* scattering, as $K_g/K_l \ll 1$. The resulting cross-section is the "hard sphere" Rayleigh limit

$$\sigma_{sc}^{Ra} = \frac{4\pi}{9} \frac{R_0^6 \omega_d^4}{c_l^4}. \qquad (28)$$

In analogy to the case of the "soft sphere" above, the resonance peak is shifted to arbitrarily *large* radii for an arbitrarily stiff bubble, so that here (28) is valid for every finite R_0.

3.5 The regime of ultrasound diagnostics

It is important to note that for the typical μm size bubbles of ultrasound diagnostics applications, the relevant limiting cases of the linear formulas (20, 21) are equations (24, 26, 27). The case of $\sigma_{sc}^{lin} \propto R_0^6$ given by (22) does not occur, because the resonance radii R_0^{res} are – for MHz driven bubbles – in the range of the crossover ambient radius $R_0 \approx 0.96\,\mu\mathrm{m}$ between gas pressure and surface tension dominated resonances. Thus, the oscillations of bubbles with $R_0 < R_0^{res}$ are all surface tension dominated, and never show the R_0^6 behavior. This is obvious in Figure 2, which shows the linear cross-sections for 3 MHz driven bubbles in blood. In contrast to Figure 1, there is a direct transition from the resonance peak to a curve $\sigma_{sc}^{lin} \propto R_0^8$.

3.6 Linear absorption cross-sections

The linear analysis is naturally extended to absorption cross-sections; the analytical formula for σ_{abs}^{ν} in the case of monochromatic driving is easily found *via* (14) and (17–19) to be

$$\sigma_{abs}^{\nu,lin} = \frac{16\pi\nu_l c_l}{R_0} \frac{\omega_d^2}{(\omega_0^2 - \omega_d^2)^2 + 4\gamma^2\omega_d^2}. \qquad (29)$$

Here, the limiting cases for small bubbles show $\sigma_{abs}^{\nu,lin} \propto R_0^3$ for small R_0 for gas pressure dominated ω_0 and $\sigma_{abs}^{\nu,lin} \propto R_0^5$ for the surface tension dominated case (see Fig. 2). Thus, $\sigma_{abs}^{\nu,lin} \gg \sigma_{sc}^{lin}$ for small bubbles, *i.e.*, most of the energy incident on the bubble is converted into heat through viscous damping, whereas only a small part is available for sound emission. The already surprisingly high *scattering* cross-section for microbubbles is outnumbered considerably by the *absorption* cross-section. The same is true in resonance, where

$$\frac{\sigma_{abs}^{\nu,lin,res}}{\sigma_{sc}^{lin,res}} \approx \frac{4\nu_l c_l}{(R_0^{res})^3\omega_d^2} \approx 23 \qquad (30)$$

can be calculated for $f_d = 3$ MHz and the material constants of blood, in very good agreement with numerical computation (*cf.* Fig. 2).

For large R_0 above the resonance radius we have $\sigma_{abs}^{\nu,lin} \propto R_0^{-1}$; as σ_{sc}^{lin} grows like R_0^2, we have in this range $\sigma_{abs}^{\nu,lin} \ll \sigma_{sc}^{lin}$, and the major part of the energy goes into sound emission.

4 Pulsed driving

4.1 The incident pulse

One assumption that allowed us to give simple analytical formulas was the monochromaticity of the driving. In reality, bubbles in ultrasound diagnostics are driven by the signal of a diagnostic transducer, which is almost always *pulsed*, and quite often (*e.g.* in pulse wave Doppler mode) the pulses are only a few wavelengths long.

In closer agreement with experimental reality, we therefore model the pressure pulse $P(t)$ as

$$P(t) = P_a \cos(\omega_d(t - t_c)) \exp\left(-\frac{h^2\omega_d^2}{4}(t - t_c)^2\right), \quad (31)$$

centered around t_c with relative width h. We choose $h = 1/3$ here. After Fourier transform, the frequency space representation is

$$P(\omega) = \frac{P_a}{h\omega_d} \left[\exp\left(-\frac{(\omega - \omega_d)^2}{h^2\omega_d^2}\right) + \exp\left(-\frac{(\omega + \omega_d)^2}{h^2\omega_d^2}\right)\right]. \qquad (32)$$

This spectrum is (almost) Gaussian in shape; the corresponding power $\propto |P(\omega)|^2$ decays to $1/e^2$ of its maximum value within a distance of $\pm h\omega_d$ around ω_d (*cf.*
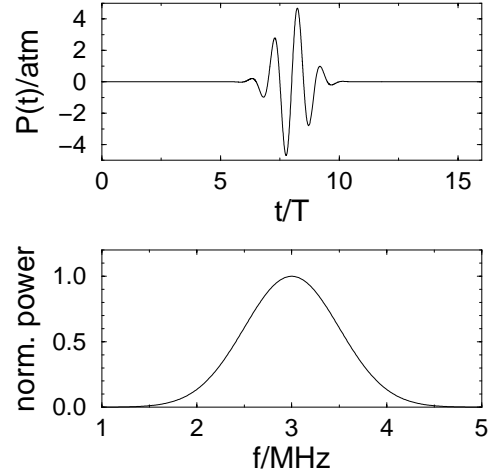
Fig. 3. Modeled ultrasound diagnostics driving pulse. The upper part of the figure shows the time series $P(t)$ (t normalized to $T \equiv 1/f_d$), the lower part the normalized Fourier spectrum of the acoustic power given by $P(t)$. It is centered around the mean frequency $f_d = 3$ MHz and decays to $1/e^2$ of its maximum value within $hf_d = f_d/3 = 1$ MHz above and below f_d. This corresponds to the effective spatial extent of the pulse of ≈ 3 wavelengths.

Fig. 3). Thus, the reciprocal $1/h$ of the relative width is an approximate measure for the spatial extension of the pulse (in wavelengths). In our example, the pulse is about 3 wavelengths long and corresponds to the shortest pulses routinely available in medical applications of diagnostic ultrasound.

4.2 Effects on the cross-sections

As we are still in the linear limit, the pulsed driving can be understood as a superposition of monochromatic waves of frequency ω with amplitudes proportional to the Fourier components $P(\omega)$ in (32). The response will be therefore obtained from a convolution of the monochromatic response discussed above and the spectrum $P(\omega)$.

Figure 4 shows the cross-sections $\sigma_{sc}(R_0)$ and $\sigma_{abs}^{\nu}(R_0)$ for monochromatic and pulsed driving in comparison. The figure is a blow-up of the region near R_0^{res}, which is the only area where there are marked differences between the responses to the different drivings. As it may have been expected, the response curves for polychromatic driving are broader, because unlike the monochromatic case, where the single frequency ω_d corresponds to a single, well-defined R_0^{res}, there are a number of R_0 for which the bubbles react strongly to the most intense frequency components in $P(\omega)$. Correspondingly, a bubble driven at resonance by a monochromatic wave is a more effective scatterer than for pulsed driving, so that the maximum height of the cross-section curves is smaller in the latter case.

Moreover, with pulsed driving there is a slight, but significant shift in the maximum of both cross-sections towards larger R_0. This is due to the asymmetry in the
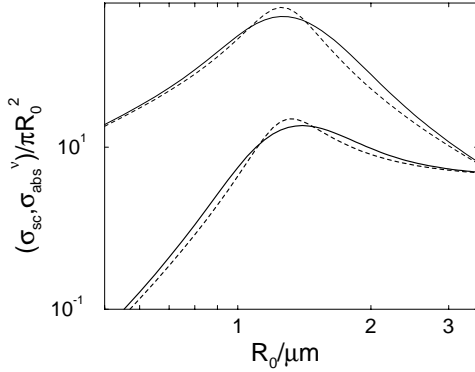
Fig. 4. Scattering (thick lines) and absorption (thin lines) cross-sections for bubbles driven by a monochromatic 3 MHz sound wave (dashed) and a diagnostic pulse according to (31) with center frequency 3 MHz (solid). The response to the polychromatic driving displays a broader, lower resonance peak, which is shifted towards larger R_0. Further away from resonance, the differences to the monochromatic case soon become negligible.

response curve around the resonance radius that is apparent already in the monochromatic case (*cf.* Fig. 4): on increasing R_0 from R_0^{res}, the cross-sections do not drop as rapidly as when R_0 is decreased from the maximum of the curves. Therefore, the contributions in $P(\omega)$ with ω slightly smaller than ω_d (which correspond to $R_0(\omega) > R_0^{res}(\omega_d)$) will have a larger effect on σ_{sc} and σ_{abs}^ν than the contributions with ω slightly smaller than ω_d, even if they are represented with the same weight in $P(\omega)$. Consequently, upon convolution of the spectrum, the cross-sections are increased for the larger R_0 and the maximum of the curves is shifted towards $R_0 > R_0^{res}(\omega_d)$.

If the width of the pulse is varied, the peak shift and peak broadening vary correspondingly: thus, if the pulse becomes very short (shorter than one wavelength), the resonance structure is almost completely lost. Using longer and longer wavetrains (smaller h), on the other hand, leads to successively sharper resonance peaks, while the repetitive oscillations of the bubble allow for the occurrence of subharmonic resonances, provided that the bubbles remain shape stable (*cf.* [6]).

5 Results of full nonlinear computations

Let us now come back to the general formulas presented in Section 2 and drop the assumption of linear response. We will find that the features of the nonlinear case can be quite different from the linear results presented above. Not surprisingly, the cross-sections now depend on the driving pressure amplitude P_a, which is not the case for linear driving. It should be noted that, in order to compare these results with experimental measurements, they have to be convoluted with the bubble size distribution, as in virtually all experiments the bubble suspensions are not monodisperse.
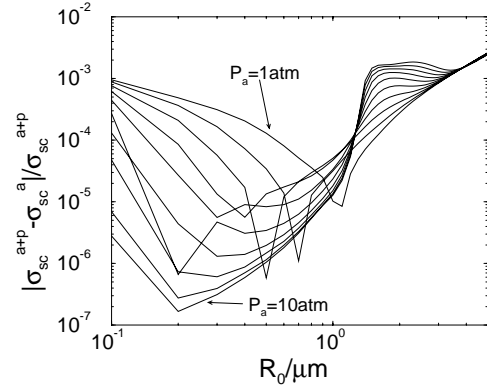
Fig. 5. Relative error of scattering cross-section computations with and without passive emission taken into account. The numerical calculations were performed using the complete formula (11) with or without the passive contribution and driving with an ultrasound diagnostics pulse according to (31). The curves correspond to driving pressure amplitudes P_a of $1-10$ atm, in steps of 1 atm. The error is nowhere greater than about 0.25%.
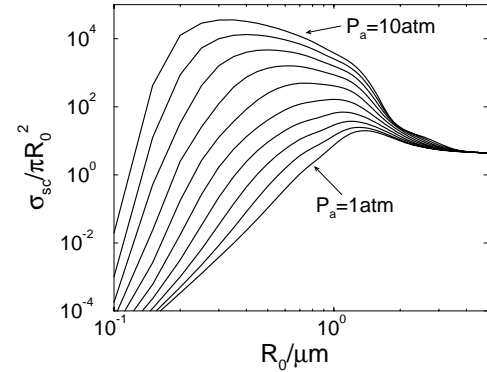
Fig. 6. Total scattering cross-sections of bubbles driven by ultrasound pulses. From bottom to top: $P_a = 1-10$ atm in steps of 1 atm. The linear profile of σ_{sc} is drastically changed for high P_a, the resonance radius shifts to smaller R_0 due to nonlinearities and the cross-sections are much larger around the resonance radius than in the linear case (up to 3–4 orders of magnitude).

5.1 Scattering cross-sections

With $P(t)$ given by (31), I_{inc} can be computed, so that with equations (1, 6, 7–9), σ_{sc} results. Let us first convince ourselves that the passive part of (1) is tiny in the nonlinear case, too. In Figure 5 we present the *relative errors* made in determining scattering cross-sections from $P_s^a(r,t)$ (or $q_s^a(t)$) alone rather than from the full interference formula (11). It is easy to see that these errors are nowhere greater than about 0.25%, and in most cases much smaller. The huge advantage of (actively emitting) bubbles as scatterers compared to stiff solid bodies of similar size is here once more strikingly demonstrated. For computational simplicity, the cross-sections presented in the following figures were computed using only the active emission part.

Figure 6 shows the normalized cross-sections for various $R_0 \in \{0.1\ \mu\mathrm{m},\ 5.0\ \mu\mathrm{m}\}$ and $P_a = 1-10$ atm (in 1 atm intervals). These values represent typical bubble sizes found in diagnostic bubble suspensions (often the size distribution shows a peak around $R_0 \approx 1\ \mu\mathrm{m}$ [1]) and typical sound pressure amplitudes in the focus of clinical ultrasound devices. From linear analysis, we know what the cross-sections for $P_a \to 0$ look like. This curve is readily reproduced for small P_a. While the curve for 1 atm is still essentially unaltered compared to the linear case, there are dramatic changes in $\sigma_{sc}(R_0)$ with higher P_a. E.g., the resonance radius R_0^{res} undergoes a shift away from its linear value to smaller R_0, i.e., in the opposite direction of the shift induced by the polychromatic pulse. This shift is explained by the nonlinearity of the oscillator (cf. [26]): when expanding the RP equation up to nonlinearities of third order, one obtains for the nonlinear eigenfrequency

$$\omega_0^{NL} = \omega_0 + a^2 \left(\frac{3\beta}{8\omega_0} - \frac{5\alpha^2}{12\omega_0^3} \right), \qquad (33)$$

with the amplitude a of the oscillation and

$$\alpha = - \left(2\omega_0^2 - \frac{2\zeta}{\rho_l R_0} \right), \quad \beta = \frac{10}{3}\omega_0^2 + \frac{14\zeta}{3\rho_l R_0}. \qquad (34)$$

It is easy to see that with these values we always have $\omega_0^{NL} < \omega_0$, i.e., the bubble is an oscillator with a *soft* potential. With stronger nonlinearity, ω_0^{NL} becomes smaller for a given R_0; in order to be in resonance, we require $\omega_d = \omega_0^{NL}$ with constant ω_d. Therefore, R_0 must be *decreased* in order to increase ω_0 beyond ω_d to ensure that the resonance condition $\omega_d = \omega_0^{NL}$ is again fulfilled. Thus, the nonlinear resonance radius $R_0^{res,NL}$ is smaller than its linear counterpart. Note also that the resonance structure is blurred especially for high driving; this is in contrast to the case of monochromatic driving [6], where well-defined resonance radii can be recognized up to the highest P_a.

A most striking feature of Figure 6 is the tremendously enlarged scattering cross-section, especially at radii smaller than the linear resonance radius (i.e., in the region of nonlinear resonance). Sometimes, σ_{sc} is greater by several orders of magnitude compared to the linear case (note the logarithmic scale). Only for $R_0 \gg R_0^{res,lin}$ is the shape of the curve virtually unaltered. Thus, the scattering cross-sections for *small* bubbles (below $\approx R_0 = 1\ \mu\mathrm{m}$) are severely *underestimated* by the linear theory.

The reason for this effect is found in the typical $R(t)$ radius dynamics of nonlinearly driven bubbles: when P_a is sufficiently high, they undergo violent *collapsing* instead of just a smooth oscillation. This leads to high velocities and extraordinarily high accelerations of the bubble wall, exceeding $10^9 g$ in the solutions of (6) for the highest P_a of our study (even larger accelerations are known in other contexts of bubble dynamics, see [19]). These values of $\dot{R}$ and especially $\ddot{R}$, which far exceed those expected for linear response, lead to very high active emission pressures (cf. Eq. (3)) and thus to a huge σ_{sc}.
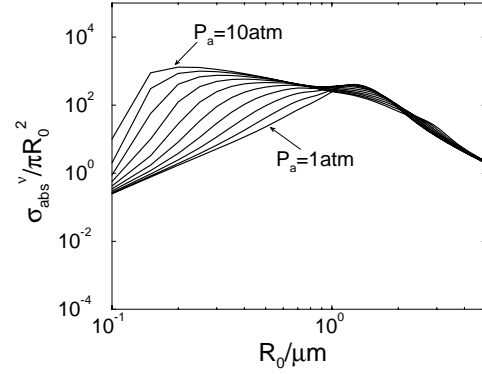
Fig. 7. Total viscous absorption cross-sections of bubbles driven by ultrasound pulses. From bottom to top: $P_a = 1-10$ atm in steps of 1 atm. The change in shape with growing P_a is not as drastic as for the scattering cross-sections. σ_{abs}^{ν} is considerably smaller than σ_{sc} for the highest P_a, while it is much larger in the linear case of small driving.

5.2 Absorption cross-sections

In Figure 7 the viscous absorption cross-section σ_{abs}^{ν} computed from equations (13, 14) is shown for the same parameter combinations as for σ_{sc} in Figure 6. As expected, the resonance peak undergoes similar nonlinear shifting. However, although σ_{abs}^{ν} also shows a tendency to grow for higher P_a, it is obvious that its dependence on driving pressure amplitude is nowhere near as dramatic as in the case of the scattering cross-section. This is because in the computation of W_{dis}^{ν} via (13), only the velocity $\dot{R}$ is present, but not the acceleration, which is responsible for the tremendous sound emission, as argued in the previous section. As usual, the radiative processes are connected with acceleration, while the dissipative processes are governed by velocity. For high P_a we can therefore conclude that – regardless of the size of the bubble – most of the incident sound energy is scattered again into sound, and not dissipated via viscous forces.

5.3 Secondary absorption

It is tempting to conclude that for the highest P_a we have the optimal situation for detection of scattered sound. This is not necessarily so, however, because of the *spectrum* of the emitted acoustic radiation. We show in a separate paper [9] that the most strongly driven bubbles emit sound in a spectrum of immense band width, with a large portion of the energy in the ultra high frequency part (GHz). These frequencies are readily absorbed (on a length scale of cm or less) by water or other media (blood, tissue) frequently encountered in diagnostic applications (cf. e.g. [27,28]). With this absorption, most of the sound energy is converted into heat. Figure 8 shows the example of the *effectively* detected scattered sound after the pulses have traveled through a 5 cm layer of water. The absorption properties of water are well known: the energy contained in every Fourier component (frequency $f = \omega/2\pi$)
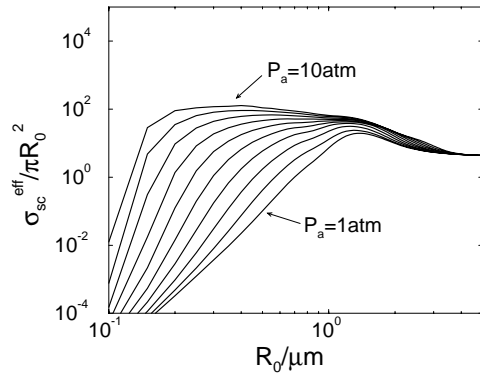
Fig. 8. Effective scattering cross-sections of bubbles driven by ultrasound pulses and separated from the detector by a water layer of 5cm width, which acts to damp out high frequency sound according to (35). From bottom to top: $P_a = 1-10$ atm in steps of 1 atm. The growth for large P_a is much diminished here as compared to Figure 6. The high frequency components of the sound emitted by the small bubbles at high P_a are absorbed in water and thus the major part of the emitted sound energy is lost to the detector.

of the emitted sound signal decays over a distance r like

$$E_s(r, f) = E_s(0, f) \exp(-\alpha_w f^2 r), \qquad (35)$$

with the known characteristic absorption coefficient of water $\alpha_w \approx 1.5 \times 10^{-14}$ s^2/m [29]. Thus, the highest frequency components experience the strongest damping, and it is especially the high-power, high-frequency emission of scatterers at small R_0 which is radically diminished by this process, although the cross-sections do not drop to or near their linear values. The implications for diagnostics, such as possible risks of the heat deposition connected with the absorption, are dealt with in separate work [9].

6 Summary and conclusions

We have presented a unified view of gas bubble sound scattering and absorption. Starting from the description of the bubble as a nonlinear oscillator, general formulas have been developed that can be shown to transform, in certain limiting cases, into a number of apparently discrepant formulas found in literature, whether they be derived from oscillator theory [4], scattering theory [5] or the theory of solid body sound scattering [3]. It is important to state that there is *no antagonism* between "scattering" and "active sound emission". Both terms refer to the sound that can be detected after incident sound has hit a gas bubble. The total scattering cross-section does contain a contribution of *passive* sound emission, but this contribution is tiny and can always be neglected for situations in ultrasound diagnostics. Bubbles driven in the *nonlinear* range show a *much larger* scattering cross-section than in the linear case and are more "actively" emitting sound in the sense that the incident energy is primarily converted into sound and not into viscous heating, as is the case for linear driving. The most prodigiously radiating bubbles, at small radii and large driving amplitude, emit such high frequency sound that it is again absorbed by the surrounding medium and leads to secondary heating. The effective

yield of scattered sound energy is therefore much smaller than what would be expected without taking absorption into account. Still, the ultrasound scattering capabilities of bubbles and therefore their effectiveness as a contrast agent in diagnostics are considerably enhanced due to the nonlinearity of the oscillations.

References

1. See the articles in *Advances in echo imaging using contrast enhancement*, edited by N.C. Nanda, R. Schlief (Kluwer Academic Publishers, Dordrecht, 1993).
2. R. Gramiak, P.M. Shah, Invest. Radiol. **3**, 356 (1968).
3. L.D. Landau, E.M. Lifshitz, *Fluid Mechanics* (Pergamon Press, Oxford, 1987).
4. T.G. Leighton, *The acoustic bubble* (Academic Press, London, 1996).
5. R.Y. Nishi, Acustica **33**, 65 (1975).
6. S. Grossmann, S. Hilgenfeldt, D. Lohse, M. Zomack, J. Acoust. Soc. Am. **102**, 1223 (1997).
7. A. Prosperetti, J. Acoust. Soc. Am. **56**, 878 (1976).
8. A. Prosperetti, J. Acoust. Soc. Am. **57**, 810 (1975).
9. S. Hilgenfeldt, D. Lohse, M. Zomack, *Scattering and heat deposition of pulse-driven microbubbles*, preprint (1998).
10. C.E. Brennen, *Cavitation and Bubble Dynamics* (Oxford University Press, Oxford, 1995).
11. Lord Rayleigh, Philos. Mag. **34**, 94 (1917).
12. F.R. Gilmore, Hydrodynamics Laboratory, California Institute of Technology, Pasadena, report **26-4**, (1952).
13. H.G. Flynn, J. Acoust. Soc. Am. **58**, 1160 (1975).
14. J.B. Keller, M.J. Miksis, J. Acoust. Soc. Am. **68**, 628 (1980).
15. G.J. Lastman, R.A. Wentzell, J. Acoust. Soc. Am. **69**, 638 (1981).
16. G.J. Lastman, R.A. Wentzell, J. Acoust. Soc. Am. **71**, 835 (1982).
17. A. Prosperetti, J. Fluid Mech. **222**, 587 (1991).
18. A. Prosperetti, in *Bubble dynamics and interface phenomena*, edited by J. Blake, *et al.* (Kluwer Academic Publishers, Dordrecht, 1994), p. 3.
19. B.P. Barber, *et al.*, Phys. Rep. **281**, 65 (1997).
20. H. Landolt, R. Börnstein, *Zahlenwerte und Funktionen aus Physik und Chemie* (Springer, Berlin, 1969).
21. M. Plesset, A. Prosperetti, Ann. Rev. Fluid Mech. **9**, 145 (1977).
22. S. Hilgenfeldt, D. Lohse, M.P. Brenner, Phys. Fluids **8**, 2808 (1996).
23. V. Bjerknes, *Die Kraftfelder* (Friedrich Vieweg, Braunschweig, 1909).
24. A. Prosperetti, Ultrasonics **22**, 115 (1984).
25. N. deJong, *et al.*, Ultrasonics **29**, 324 (1991).
26. L.D. Landau, E.M. Lifshitz, *Mechanics* (Pergamon Press, Oxford, 1960).
27. C.M. Sehgal, J.F. Greenleaf, J. Acoust. Soc. Am. **72**, 1711 (1982).
28. H.A.H. Jongen, J.M. Thijssen, M. van den Aarssen, W.A. Verhoef, J. Acoust. Soc. Am. **79**, 535 (1986).
29. K.F. Herzfeld, T.A. Litovitz, *Absorption and dispersion of ultrasonic waves* (Academic Press, New York, 1959).